Advanced Powder Technology 35 (2024) 104481

Contents lists available at ScienceDirect

Advanced Powder Technology

journal homepage: www.elsevier.com/locate/apt

Original Research Paper

Experimental development of packing structures in a gas-particle trickle flow heat exchanger for application in concentrating solar tower systems

Markus Reichart [a,*], Alexander Hirt [a], Jakob Technau [a], Anja Raab [a], Luka Lackovic [a], Ralf Uhlig [a], Martina Neises-von Puttkamer [c], Robert Pitz-Paal [b,d]

[a] Institute of Solar Research, Pfaffenwaldring 38-40, Stuttgart 70569, Germany
[b] Institute of Solar Research, Linder Höhe, Köln 51147, Germany
[c] Institute of Future Fuels, Im Langenbroich 24, Jülich 52428, Germany
[d] Chair of Solar Technology, Linder Höhe, Köln 51147, Germany

ARTICLE INFO

Article history:
Received 19 January 2024
Received in revised form 26 April 2024
Accepted 5 May 2024
Available online 27 May 2024

Keywords:
trickle flow heat exchanger
particle air heat exchanger
direct contact heat exchanger
particle hydrodynamics
packing geometry
packing structure
CST
concentrated solar thermal

ABSTRACT

Ceramic particles represent a viable alternative as heat transfer and storage medium in concentrating solar tower systems. The particles are heated in solar-receivers close to 1000 °C. To utilize the stored energy in the particles, an air-particle direct-contact trickle-flow heat exchanger has been identified as suitable for this task. To date, no design recommendations exist that identify an optimized packing structure capable of providing a high particle volume fraction and a uniform spatial particle density distribution for a given grain type. Consequently, an experimental selection process is presented in this work to assess various packing structures for a given grain type in a trickle-flow reactor. The experiments were conducted with countercurrent flowing air at ambient conditions and 1 mm bauxite particles. A variety of packing structures were investigated at varying media flow rates. For each flow condition, the particle volume fraction was determined, as well as the particle distribution in a separate analysis. The cold experiments yielded a clear image of a preferred packing geometry, which will be discussed in detail. The results will serve as the basis for further hot experiments and thermal performance analysis in future work, where the packing geometry can be refined iteratively if necessary.

1. Introduction

Research activities in the field of Concentrated Solar Thermal (CST) applications are often motivated to enhance competitiveness to other technologies. Today, molten salt is dominantly used as heat transfer fluid (HTF) in concentrating tower systems, which are typically limited to temperatures near 600 °C [16]. One method to improve the efficiency and applicability of CST systems is to increase the operating temperature of the fluid. HTFs based on sintered bauxite particles allow process temperatures up to 1000 °C, as the material starts to sinter at 1100 °C [3]. A new direct-absorbing 2.5 MW_{th} particle centrifugal receiver system was developed and demonstrated at the Juelich Solar Tower, with particle outlet temperatures up to 965 °C under on-sun conditions [2]. To further develop particle-based CST and CSP technologies toward commercial application, the heat of the particles must be transferred to a working fluid, such as air, to provide solar heat for industrial processes (SHIP) or for power generation. Typical state-of-the-art technologies for gas-particle interaction include fluidized bed (FB) or cyclone (CY) reactors or heat exchangers (HX). For operation in a CST application, a compact volume is preferred to place the HX ideally close to the solar receiver in the solar tower. This configuration is intended to minimize heat losses and insulation costs. Furthermore, a low pressure drop is desired to keep the operation cost of the air blower low. In the FB, the gas flow must be at least high enough to lift the weight of the particles to achieve particle fluidization at the expense of a corresponding pressure drop [5]. Conversely, the volume of the CY-HX, which is typically employed in the mining and cement industries with heights exceeding 50 m [7], would not be sufficiently compact. Furthermore, CY-HX would necessitate a substantial volume of insulation to maintain heat losses at an acceptable level. A gas-particle trickle flow direct-contact heat exchanger (TFHX) is regarded as a promising alternative to the state-of-the-art technologies. Typically, the gas-particle trickle flow reactor is employed in the food or process industries for drying or chemical processes. Previous studies have described and confirmed the capacity for high heat transfer

* Corresponding author.
E-mail address: markus.reichart@dlr.de (M. Reichart).

https://doi.org/10.1016/j.apt.2024.104481

Nomenclature

List of Symbols

a	m_p^2/m_{HX}^2	specific particle surface per m_{HX}^2
A	m^2	surface area
β	m_p^3/m_{void}^3	particle hold-up
β^*	m_p^3/m_{HX}^3	extended particle hold-up
c_p	$J/(g \cdot K)$	specific heat capacity const. pressure
d	m	diameter
ϵ_0	m_{void}^3/m_{HX}^3	volumetric packing void fraction
$\vec{g}$	m/s^2	gravitational acceleration
h	m	height
$\dot{m}$	kg/s	mass flow
n	–	number
P	–	mixing composition of two quantities
σ_0^2	–	segregated mixture
σ_{id}^2	–	ideal mixture
σ_z^2	–	stochastic uniform mixture
ρ	kg/m^3	density
t	m	thickness
u_{rel}	–	relative linear particle distribution
u_n^2	–	mixing quality of two quantities
$[var]$		uncertainty
V	m^3	volume
w	m	width
X	–	sample mixing composition
z	m	vertical distance

Subscripts and Superscripts

#	$[var]/m^2$	normalized to A_{HX}
a	air	
A	component A	
bar	packing bar element	
B	component B	
dyn	dynamic	
f	free	
p	particle	
pac	packing	
s	sphere	
S	Sauter	
sm	sheet metal	
stat	static	
ts	tray support	
tot	total	
void	void space	

Abbreviations

CSP	concentrated solar power
CST	concentrated solar thermal
CY	cyclone
DEM	discrete elements method
FB	fluidized bed
HTF	heat transfer fluid
HX	heat exchanger
PU	packing unit
SM	sheet metal
SHIP	solar heat for industrial processes
TFHX	trickle flow heat exchanger
TS	tray support

capabilities in analogy to mass transfer in trickle flow reactors [19]. Building upon previous work that has explored temperatures up to 400 °C [19,8], the TFHX concept will be further developed in this present study. The existing literature provides data on the gas-particle trickle flow reactor and the corresponding hydrodynamic behavior of gravity-driven particle flow within the packing structure, with and without countercurrent air flow [22,14,13,20,4,6]. Other work has focused on unstructured packings such as dumped Pall or Raschig rings [22,14,13]. Additionally, structured packings with regularly arranged packing elements, such as round or rhombus-shaped geometries, have also been investigated. Verver and van Swaaij [20] demonstrated that irregular packing structures are more prone to particle segregation, resulting in the formation of visibly thick strands of trickling particles, which leads to an uneven particle density distribution within the packing void. Additionally, they observed that regular packing structures exhibit a higher particle volume fraction in the packing void and a lower pressure drop in the countercurrent gas flowing upward. Despite the extensive hydrodynamic investigations documented in the literature, no systematic approach for the selection of a favorable packing geometry has been identified. Solely Verver and van Swaaij [20] mention their motivation for rotating the squared bar elements by 45° parallel to the horizontal bar axis as a means of avoiding particle accumulation [20]. A high particle volume fraction or hold-up, β, is preferred since it correlates proportionally with the volume specific particle surface within the packed column, a_p, see (7), that participates at the gas-particle interaction. Correspondingly, to use a trickle flow reactor in heat exchanger operation, it is desirable to increase a_p, to enhance the gas-particle heat transfer rate and consequently increase the volumetric power density. An increase in power density allows a heat exchanger with the same power level to reduce its volume, thereby reducing thermal losses to the environment. Another design criterion for heat exchanger operation is a uniform particle distribution of the flowing grains within the packing structure in the TFHX to avoid particle segregation. This criterion was previously investigated in a simulation model by Reichart et al. [12] and also in a separate measurement procedure in this study. A test rig was constructed for the purpose of developing a trickle flow heat exchanger. This setup allowed for the conduction of cold test campaigns, during which the grain flow behaviour of a specific particle type within different packing geometries was examined. The focus of this research was to identify a packing geometry that would be most effective in meeting the aforementioned packing design criteria.

2. Materials and methods

In the following the characterization methods and the defined labeling syntax for packing geometries are outlined. Also, the calculation of the particle volume fraction within the packing is derived and the characteristics of the used particles is presented.

2.1. Packing geometry

A uniform particle density distribution is desired while the particles trickle downwards through the packing structure of the HX. As described above and demonstrated in previous work [12], horizontal packing layers with a number of equally spaced bar elements, n_{bar}, will be used to assemble the packing structure. The packing layers are stacked with staggered and non-staggered layers. In previous work [4,19] each packing layer was rotated

alternately 90° parallel to the axis of gravity, the reasons for this not being outlined. The arrangement of the bar elements in this work is chosen slightly different, see Fig. 1, by stapling one staggered and one non-staggered packing layer directly on top of each other and collinear aligned. This arrangement of two packing layers is repeated vertically by alternately rotating the group of layers 90° parallel to the axis of gravity. After four packing layers, the sequence of layer is repeated, and form one packing unit (PU).

This arrangement was used in this study, since it was observed qualitatively that the particles form particle curtains when falling from a non-staggered packing layer to a collinear aligned staggered packing layer. This mimics multiple times a zigzag contactor, forcing the countercurrent flowing gas to pass the particle curtains, resulting in a high gas-particle interaction and hence high capabilities for heat and mass transfer [11,10]. A further advantage of the used packing arrangement is that the probability of the trickling particles to hit a bar element in the packing layer below increases. This causes a decrease of the mean particle sink velocity in the packing structure, $\bar{u}_p$, and an increase of the dynamic particle hold-up, since β is proportional to $\bar{u}_p^{-1}$, see (7). To uniquely identify the different packing geometries, a concatenation of the following parameters is used to label the geometries: bar width w_{bar} in mm, bar height h_{bar} in mm, number of horizontal bar elements in a non-staggered packing layer n_{bar} and the particle falling height z in mm. Fig. 1 shows the labeling for an exemplary packing geometry with rectangular bar elements that can be named accordingly to "w04 h04 n4 z10". When designing different packing geometries, it has to be considered that the resulting void spacing between the horizontal bar elements in a packing layer, w_{void}, should not be chosen too small, to prevent the moving particles from clogging and flooding the HX with particles. As a rule of thumb, it is advised to design openings with at least 10-times the particle diameter to prevent particles from clogging [23]. During the experiments, it was observed, that for the setup in this work, a void spacing of 6 times the particle diameter provided reliable particle flow. Individual geometric parameters are used to describe the packing geometry. For a certain bar width and number of elements per packing layer w_{void} can be calculated for the width of the HX channel, w_{HX}.

$$w_{void} = \frac{w_{HX}}{n_{bar}} - w_{bar} \tag{1}$$

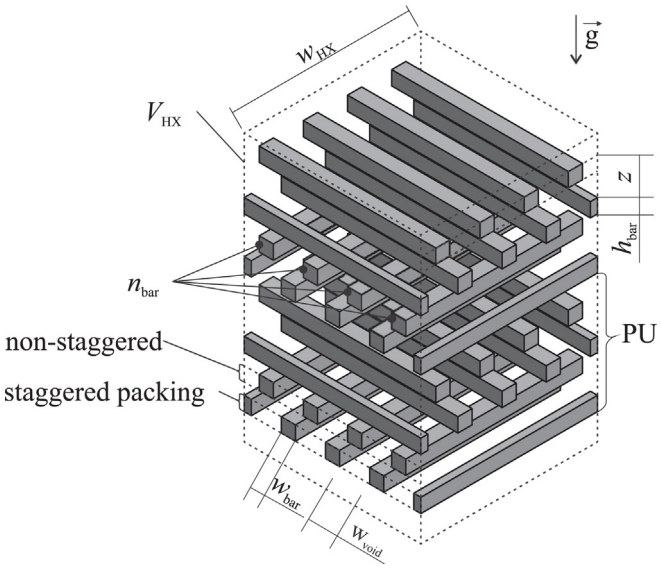

Fig. 1. Exemplarily packing arrangement, with geometrical parameters.

The effective packing porosity, ϵ_{eff}, is the void area within a packing layer, A_{void}, normalized to the free cross-sectional area of the heat exchanger channel without packing structure, A_{HX}. Whereas A_{void} can be determined by subtracting the projected packing surface of a bar layer, A_{pac}, from the cross-sectional area of the HX channel, A_{HX}.

$$A_{void} = A_{HX} - A_{pac} = w_{HX}^2 - w_{HX} w_{bar} n_{bar} \tag{2}$$

$$\epsilon_{eff} = \frac{A_{void}}{A_{HX}} = \frac{A_{HX} - A_{pac}}{w_{HX}^2} = 1 - \frac{w_{bar} n_{bar}}{w_{HX}} \tag{3}$$

Similarly, the packing void fraction or packing porosity, ϵ_0, is the total void volume within the packing structure, V_{void}, normalized with the volume of the heat exchanger, V_{HX}.

$$V_{void} = V_{HX} - V_{pac} = w_{HX}^2 h_{HX} - V_{pac} \tag{4}$$

$$\epsilon_0 = \frac{V_{void}}{V_{HX}} \tag{5}$$

2.2. Particle hold-up

As mentioned, it is mandatory to know the particle volume fraction, or particle hold-up, for the assessment and its applicability of different packing structures in a TFHX. A high particle hold-up increases the specific particle surface, a_p, that participates at the heat transfer. a_p is the surface of all particles within the packing void, normalized to the HX volume, V_{HX}. The calculation of a_p is based on the definition of the volume specific surface of a sphere a_S, which is derived from the Sauter diameter, d_S.

$$a_S = \frac{6}{d_S} \tag{6}$$

By multiplying a_S by the particle hold-up and the packing porosity, the specific particle surface area can be calculated for all particles in the TFHX, where $V_{p,pac}$ is the total volume of all particles in the packing structure as a product of the total particle number in the packing and the single particle volume, $V_{p,pac} = n_{p,pac} V_p$.

$$a_p = a_S \beta \epsilon_0 = \frac{\sum A_p}{V_{p,pac}} \frac{V_{ppac}}{V_{void}} \frac{V_{void}}{V_{HX}} = \frac{A_{p,pac}}{V_{HX}} = \frac{6}{d_p \beta \epsilon_0} = \frac{6 \dot{m}_p^{\#}}{\rho_p d_p} \frac{1}{\bar{u}_p} \tag{7}$$

If the averaged particle sink velocity, $\bar{u}_p$, is known, a_p can be determined using the particle density, the particle diameter, and mass flow rate of the particles, $\dot{m}_p^{\#}$, normalized to A_{HX}. The particle hold-up represents the fractional volume of the sum of all particles within the packed column, $V_{p,pac}$, normalized by the packing void volume, V_{void}.

$$\beta = \frac{V_{p,pac}}{V_{void}} = \frac{m_{p,pac}/\rho_p}{V_{HX} \epsilon_0} \tag{8}$$

A general approach to calculate β is defined by (8), however the particle hold-up can be broadly distinguished between static particles, β_{stat}, resting on the packing structure, and dynamic particles freely trickling in the packing, β_{dyn}, see Fig. 2. Similarly, a_p also can be determined for each state of motion (total, dynamic or static).

$$\beta_{tot} = \beta_{dyn} + \beta_{stat} \tag{9}$$

A more detailed subdivision of the different flow regimes is described by Westerterp and Kuczynski [22] but it is not preserved as necessary for the scope of this work. It is assumed that the fraction of particles that is predominantly involved in the gas-particle heat transfer is provided by the trickling particles, represented by the dynamic hold-up, β_{dyn}, [18]. Therefore, if not mentioned other-

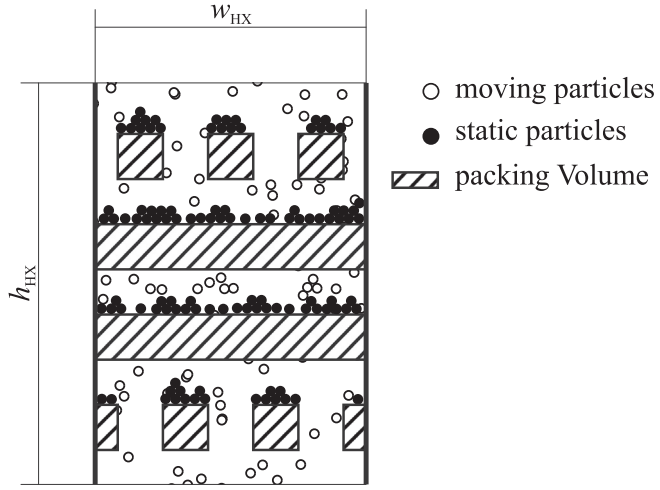

Fig. 2. Moving and static particles within staggered packing type.

wise, all references to particle hold-up will be to dynamic particle hold-up, unless otherwise stated.

In the work available in literature, focusing on the particle hydrodynamics within packing structures, the packing geometry itself is not changed, resulting in V_{void} as a constant referable value suitable for normalization. In the present work, the void structure and correspondingly ϵ_0 can vary substantially with changing packing geometries, why in this study the extended particle hold-up, β^*, is defined with respect to the heat exchanger volume, V_{HX}, with the following relationship between β and β^*:

$$\beta^* = \frac{V_{p,pac}}{V_{HX}} = \beta\epsilon_0 \tag{10}$$

With alternating packing structures V_{HX} remains constant, allowing it to compare different geometries, by using β^*.

2.3. Particle density distribution

For an optimized gas-particle interaction and corresponding heat transfer in the TFHX, a high grade of mixing between the two phases is desired. The spatial distribution of a grain system can be expressed by the mixing quality of two components A and B. Where for instance A represents the volume fraction of the trickling particles and B is set equal to the void fraction filled with air and the volume of the packing structure. The mixing quality is determined by the mean square deviation of the empirical variance, u_n^2, of n samples X_i for a known total mixture composition P of the components A and B [17].

$$u_n^2 = \frac{1}{n} = \sum_{i=1}^{n}(X_i - P)^2 \tag{11}$$

$$P = \sum_{i=1}^{n} X_i = \frac{\sum_{i=1}^{n} V_{A,i}}{\sum_{i=1}^{n} V_{sa,i}} = \sum_{i=1}^{n} \frac{V_{A,i}}{V_{sa,i}} \tag{12}$$

The mixing quality or particle density distribution, u_n^2, is compared to the limited nature of mixtures, described by a completely segregated mixture, σ_0^2, and an ideal uniform mixture, σ_{id}^2, which can be considered as a particle system where all components are perfectly equally spaced and distributed. However, since this theoretical case for σ_{id}^2 cannot be achieved by means of a mechanical mixing processes, in the practical application the best achievable mixing quality can be described by the stochastic uniform mixing, σ_z^2, see Fig. 3.

$$\sigma_0^2 = P(1-P) \tag{13}$$

$$\sigma_{id}^2 \equiv 0 \tag{14}$$

$$\sigma_z^2 = \sigma_0^2 \frac{V_A}{V_{sa}} \tag{15}$$

In previous work the relative linear particle distribution, u_{rel}, was defined to directly compare the determined mixing quality to its extrema [12].

$$u_{rel} = \frac{\sqrt{u_n^2} - \sqrt{\sigma_z^2}}{\sqrt{\sigma_0^2} - \sqrt{\sigma_z^2}} \tag{16}$$

To assess the quality of mixing between particles and air, an optical measurement method was developed and applied. The definition of u_{rel} will be used in this work to evaluate the mixing quality of the particle flow within different geometries. The method is applied by using a consumer camera setup consisting of a Tokina FIRIN 100 mm macro lens and a Sony Alpha ILCE-6400 camera with video function. Videos have been made and analyzed during a separate campaign. For those tests an observation area free of packing elements was created in the packing structure to assess the development of the freely falling particles and to determine the quality of spatial distribution of the particles. For the campaign transparent walls were installed to observe the particle flow within the packing structure and the observation area. The narrow vertical distance between two packing layers and the resting particle piles on the packing elements, see Fig. 4 (right), disturbed the analyzation of the particle mixing quality, see Fig. 4 (right). Therefore, the assessment of the particle mixing was performed in a separate observation area. Fig. 4 (left) shows an illustration of the trickling particles within the packing structure. It can be seen that depending on the orientation of the packing elements, only areas with a rather opaque curtain of particles can be observed, not allowing to assess in depth the particle density distribution. However, it is assumed that the grain distribution within the packing elements rotated by 90° will be similar to the particle trajectories, caused by packing layers with a colinear alignment of the bar elements to the camera optics. Accordingly, the free space of the observation area was selected below a packing layer with colinear bar elements to the camera optics, to observe the influence of bar width and the development of shaded areas, causing an undesired unevenly distribution of particle density in space, see Fig. 4 (left). It is assumed that the influence of shading and uneven particle distribution takes place below every packing layer within the packing structure, whereas a less pronounced effect as in the observation area is expected, since the particles have less falling height to develop its trajectories. However, it is presumed, that for a relative assessment of particle distribution within different packing structures this approach is feasible.

Fig. 5a shows an exemplarily frame of an analyzed video, before and after subdividing the frame in n subsections, see Fig. 5b, for the determination of X_i and u_n. It can be seen that in the clear image (left) and the rasterized image (right) the three particle streams can be observed, caused by the installed "w14 h02 n2 z10" packing structure.

Uncertainty analysis showed that a mixing quality of 50 frames for each video has to be averaged to obtain statistical significance. The described measurement approach reduces a three-dimensional problem to a two-dimensional problem, entailing the uncertainty of neglecting overlapping particles along the observation depth of the camera. Since only dilute particle flow

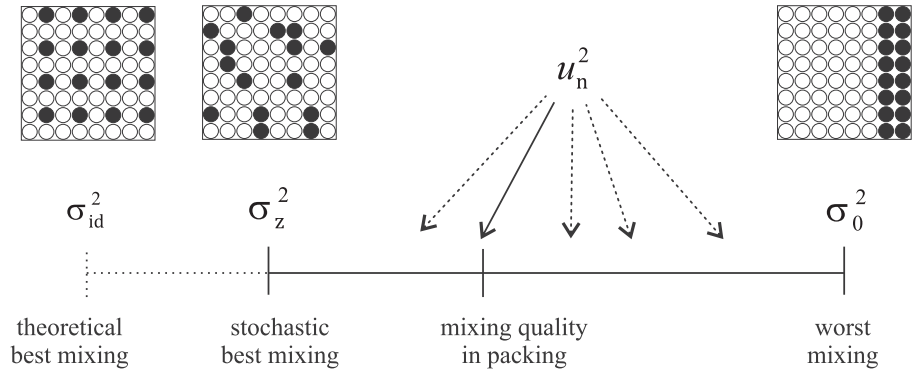

Fig. 3. Assessment quality of mixtures, [12].

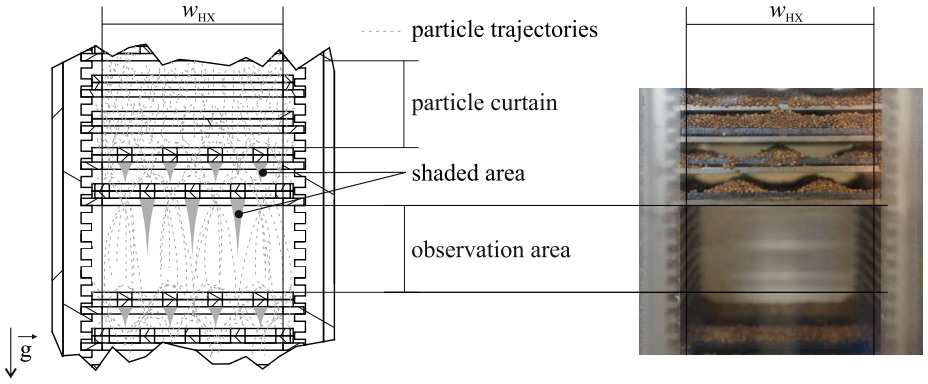

Fig. 4. Trickling particles in observation area (left) and observation area of the test setup after experiment (right).

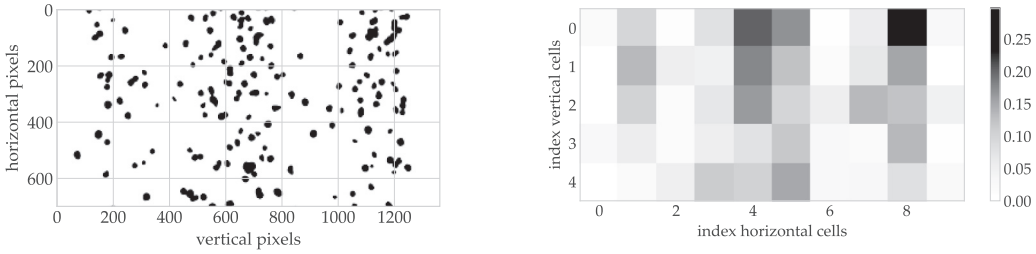

(a) Cleaned video frame of falling particles in free space

(b) Mixing quality of anylized video frame for various samples X_i

Fig. 5. Exemplarily analysis of video frame in the observation area, packing: "w14 h02 n2 z10".

with a particle void fraction of approximately 1 % is observed, the risk of overlapping particles can be neglected, why the described approach for the scope of this work is considered as feasible.

2.4. Used particles

The particles in this work were chosen in accordance to a large-scale technical demonstration of a solar direct absorbing particle centrifugal receiver, where Saint-Gobain Proppants 16/30 sintered bauxite have been used [1]. The properties of the bauxite particles with approximately 1 mm in diameter are listed in Table 1.

Table 1
Properties Saint-Gobain Proppants 16/30 sintered bauxite [15].

particle size distribution	cumulative wt.%
< 0.595 mm	12
< 0.814 mm	84
< 1.190 mm	4
mean particle diameter	0.98 mm
sphericity	0.9
bulk density	2.04 g/cc

3. Experimental assessment of packing structures

As noted above, the literature indicates that an array of regular bar elements is more likely to produce a grain flow with a uniform particle distribution and higher particle retention than irregular structures. Bar elements with round, rhombus, or triangular cross-sectional areas were used in the literature [20,4,8]. However, the motivation for the choice of a certain bar shape is not mentioned explicitly in the accessible work. Using discrete element

methods, Reichart et al. [12] numerically evaluated the particle hydrodynamics of trickling particles within different packing geometries that are constituted by regularly arranged bar elements. Different packing geometries assembled by one of four different basic bar shapes with a rectangular-, rhombus-, round- or v-shaped cross-sectional area were analyzed. As a result of this simulative pre-selection process, it was found that packing structures composed by rectangular bar elements provide the highest particle hold-up at a uniform spatial density distribution in relation to the other shapes. The further development of a packing structure with optimized geometrical dimensions is outlined in this experimental section. The measurement setup and the cold testing procedure are described followed by the assessment of the particle behavior at varying media flow rates in different packing structures.

3.1. Experimental setup

During the numerical pre-selection of packing structures, idealized packing geometries are investigated such as depicted in Fig. 1. For the experimental tests, an assembly procedure was developed, allowing to install and assess different packing geometries. Fig. 6 shows an example of how an idealized arrangement of rectangular bar elements can be assembled in the experimental setup. Sheet metals (SM) with the thickness t_{sm} are laser cut to the desired width and number of bar elements per packing layer. The effective bar height, h_{bar}, for the desired packing geometry is the result of the number of staged sheet metal elements per packing layer, n_{sm}.

$$h_{bar} = n_{sm} t_{sm} \tag{17}$$

In the exemplary geometry, shown in Fig. 6 (middle and right), each packing layer consists of two packing SMs to provide a desired bar height. In order to hold the packing SMs at defined heights, empty frame SMs with the internal dimensions of w_{HX} = 50 mm and the same thickness of t_{sm} = 2 mm were used. The packing SMs can be mounted flexibly in the developed holding arrangement "tray support" (TS), consisting of two plates with a number of 176 fins, n_{ts}, opposing each other. With a vertical spacing of h_{ts} = 5 mm, a usable heat exchanger height of $h_{HX} = h_{ts}(n_{ts} - 1)$ = 875 mm is available.

The particle falling height from one packing layer to the next layer below, z, can be selected in discrete steps due to the finned structure of the TS, where $n_{ts,f}$ is the number of free tray supports between two packing layers.

$$z = h_{ts}\left(1 + n_{ts,f}\right) \tag{18}$$

Applying (17) and (18) to the definition of the void volume within the packing (4) and the packing porosity (5), A_{void} and ϵ_{eff} can be updated and rewritten accordingly to the parameters of the test setup:

$$V_{void} = w_{HX}^2 h_{HX} - \frac{w_{HX} h_{bar} n_{ts} n_{bar} w_{bar}}{1 + n_{ts,f}} \tag{19}$$

$$\epsilon_0 = 1 - \frac{n_{sm} t_{sm} n_{ts} w_{bar} n_{bar}}{w_{HX} h_{HX}\left(1 + n_{ts,f}\right)} \tag{20}$$

Fig. 7 shows the developed test rig, which allows to install different packing structures and adjust different particle and air mass flow rates. It also includes instrumentation to measure the media inlet and outlet temperatures, the mass flow rates of particles and air, the pressure drop in the heat exchanger, and the dynamic particle hold-up.

The particle mass flow is adjusted by interchangeable orifice plates, 3, causing the particles above to dam and form a moving particle bed fed by the particle-filled hopper, 1. The orifice plates are changed when the test rig is not in operation, therefore the manual particle valve of the inlet, 2, is closed and the orifice plate can be changed. Through the orifice, the particles fall down by gravity, pass the electro-pneumatically actuated particle inlet valve, 4, and enter the heat exchanger with the mounted packing, 7. The particles trickle through the HX channel and are then, by default, directed by the drainage valve, 8, into the particle silo, 14. By operating the drainage valve, 8, particles can be drained from the system during operation. A blower 12 feeds ambient air into the setup that is measured continuously before entering the heat exchanger. Special care has been taken by assembling the test bench components of the "air inlet area" airtight with respect to the heat exchanger and the components below 6, 7, 8, 10. The air leakage was quantified in a separate pretest during the commissioning of the system by pressurizing the air inlet area and recording the pressure reduction of the pressurized system over time. The air leakage did not exceed 5 % of the air flow rate and was embedded in the gas flow measurement as a function of overpressure in

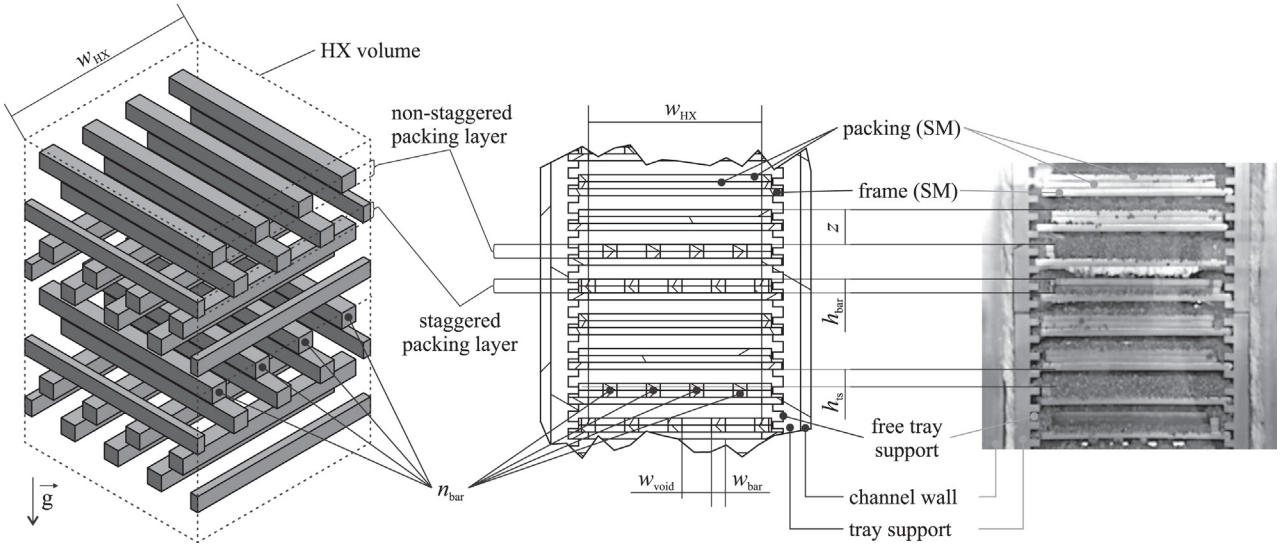

Fig. 6. Idealized packing (left), packing in experimental environment: CAD section view (middle) experimental test setup (right).

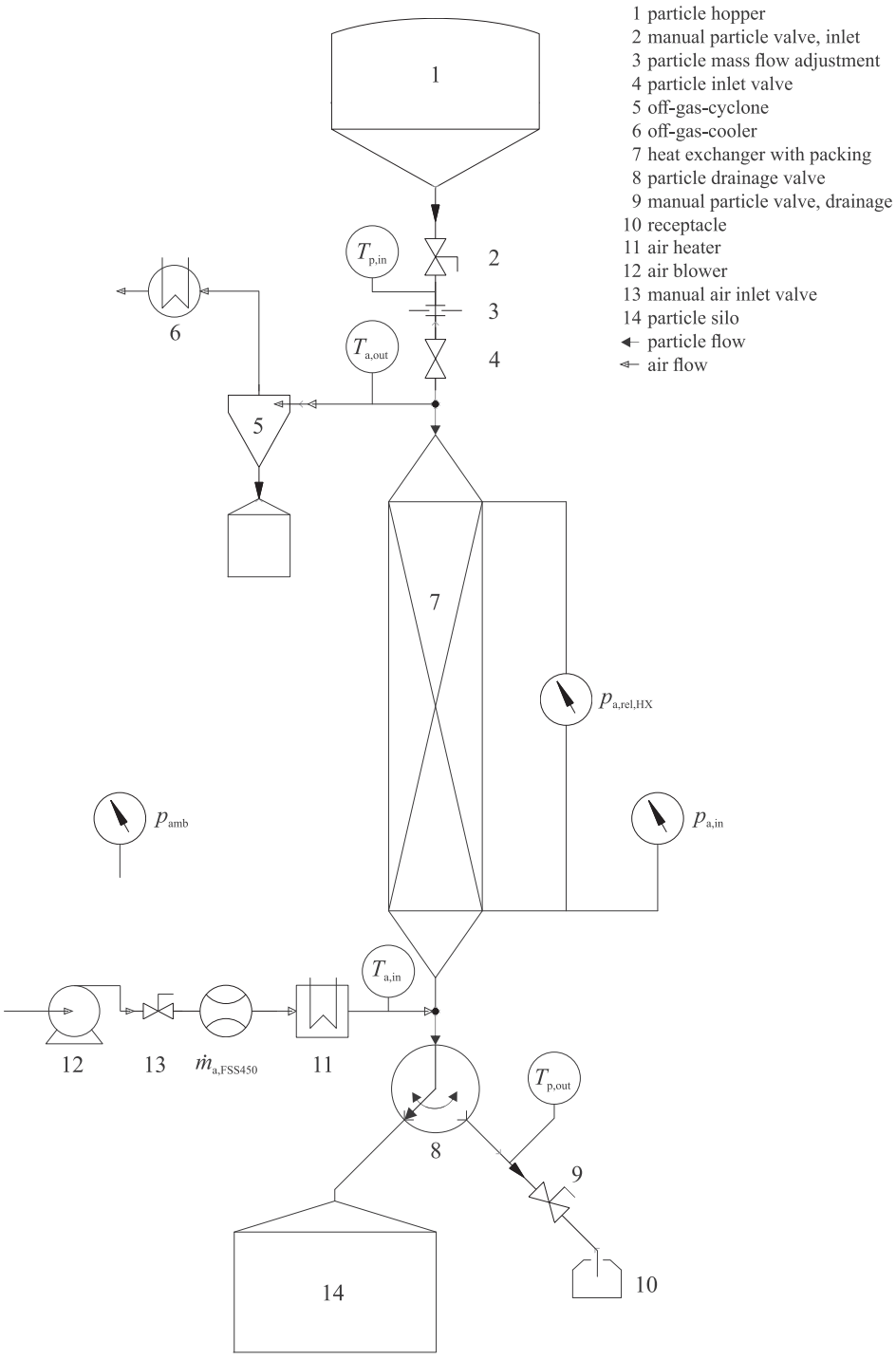

Fig. 7. Experimental set-up for the cold testing of packing structures.

the test setup with its corresponding uncertainty. The combined measurement uncertainty of the determined air flow does not exceed 3 %. The airtightness of the air inlet area forces the airflow upward through the packing structure, 7, to interact with the trickling particles. The exhaust gas leaves the system between the HX and the particle inlet valve, 4, where potentially entrained particles are separated in an exhaust gas cyclone 5. Due to the relatively narrow heat exchanger width of only 50 mm, no additional engineering measures were taken to evenly distribute the incoming particles or the gas flow. Qualitative observations and preliminary DEM and CFD simulations confirmed a uniform distribution of both media flows after entering the TFHX.

3.2. Experimental procedure

The measurement of the particle hold-up in packing structures can be done by using optical approaches with tracer particle detection [21,9] or with mechanical approaches by taking a "mechanical snapshot" of the currently trickling particle cloud within the void fraction of the packing [13,20,22]. The latter is used in this work because resting particles on the chosen rectangular packing structures would mix with tracer particles and thus falsify the measurement procedure. Once the particle flow has reached a steady state within the packing structure, the particle hold-up can be measured by simultaneously closing the particle inlet valve and opening the

drainage valve, see Fig. 7, 4 and 8. Thereby a snapshot of the free-flowing particles within the packing void is taken and collected in the drainage tube, closed by the drainage valve, see Fig. 7, 9. By opening the drainage valve, the particles can be drained out of the system. During the hold-up measurement process, the air flow is not stopped, since for gas flow rates of $\dot{m}_a^{\#} > 1\ \mathrm{kg/(s \cdot m^2)}$ it was observed that the static particles, resting upon the bar elements, start to be blown off from the bar elements, resulting in a desaturation of the static particle piles. If the gas flow were stopped during the hold-up measurement, the trickling particles would not be completely drained, as some particles would partially rain down and remain on the desaturated packing structure. This measurement method should be explicitly considered for packing structures that allow the accumulation of static particles. The drained particles represent the total amount of particles contributing to the dynamic particle hold-up. It can be expressed by the volume of drained particles, $V_{\mathrm{p,pac}}$, normalized to an appropriate reference volume. In the literature, the particle hold-up is typically normalized to the packing void volume, V_{void}, see 8. However, as described above the extended particle hold-up, β^*, is used in this work to evaluate and compare different packing structures. For each measurement of the particle hold-up the corresponding uncertainty is determined. According to 8, the uncertainty of the particle hold-up, u_β, was derived, such as for u_β^*, see (10).

$$u_\beta = \sqrt{\left(\frac{\delta\beta}{\delta m_{\mathrm{p,pac}}} u_{m_{\mathrm{p,pac}}}\right)^2 + \left(\frac{\delta\beta}{\delta \rho_{\mathrm{p}}} u_{\rho_{\mathrm{p}}}\right)^2 + \left(\frac{\delta\beta}{\delta V_{\mathrm{HX}}} u_{V_{\mathrm{HX}}}\right)^2 + \left(\frac{\delta\beta}{\delta \epsilon_0} u_{\epsilon_0}\right)^2} \tag{21}$$

$$u_\beta^* = \sqrt{\left(\frac{\delta\beta}{\delta m_{\mathrm{p,pac}}} u_{m_{\mathrm{p,pac}}}\right)^2 + \left(\frac{\delta\beta}{\delta \rho_{\mathrm{p}}} u_{\rho_{\mathrm{p}}}\right)^2 + \left(\frac{\delta\beta}{\delta V_{\mathrm{HX}}} u_{V_{\mathrm{HX}}}\right)^2} \tag{22}$$

The geometrical uncertainties $u_{V_{\mathrm{HX}}}$ and u_{ϵ_0} can be directly determined as a function of the geometric parameters of each packing structure and the HX with its corresponding individual uncertainties such as manufacturing and assembling tolerances. The uncertainty of the particle density is provided by the manufacturer. The uncertainty of the particle mass within the packing void $u_{m_{\mathrm{p,pac}}}$ is determined by considering the reading uncertainty of the drained particle mass for a number of repeated measurements and by taking into account the corresponding measurement equipment uncertainty. Also, additional measurement errors for $m_{\mathrm{p,pac}}$ are considered caused by the free falling heights between the particle inlet valve and the heat exchanger, such as between the HX and the drainage valve, and also the closing times of both actuating valves. A detailed description of the performed uncertainty analysis is omitted in this work.

4. Results and discussion

The in Section 3 described test rig was designed with great emphasis to be able to assemble a wide variety of different packing structures. In this section, the results of three experiments are presented, see Table 2, which build on each other.

4.1. Comparison of different packing geometries without gas flow

For the following comparison of different packing geometries, a particle mass flow rate of $\dot{m}_{\mathrm{p}}^{\#} = 2\ \mathrm{kg/(s \cdot m^2)}$ was used. This flow rate was derived for the case of the air superficial velocity in the empty HX duct matching the particle sink velocity at the envisioned operation temperatures of approximately 900 °C: $\dot{m}_{\mathrm{a}}^{\#} \approx 4\ \mathrm{kg/(s \cdot m^2)}$. Applying this criterion within the void spaces of the packing layers by assuming $\epsilon_{\mathrm{eff}} \approx 0.5$, the limiting air flow reduces accordingly to $2\ \mathrm{kg/(s \cdot m^2)}$. If furthermore preferably equal heat capacity flows of air and particles are assumed, the corresponding particle flow equals the air flow rate. The measurement campaign was initiated with resembling structures to the geometries investigated in the numerical preselection [12] by measuring the particle hold-ups for different design configurations of width, height, number of bars and falling height shown in Fig. 8a. Using the particle hold-up normalized to V_{void}, the figure shows a relatively high value of β for "w12 h12 n3 z15", which can be explained by the relatively low void volume compared to the other evaluated structures. This underlines the above-mentioned approach to compare different packing structures on the same basis, such as V_{HX}, and to use β^* instead of β. Furthermore, "w12 h12 n3 z15" shows a notable high uncertainty in the measured hold-up. This can be explained by the way the packing structure is installed in the test rig. By assembling the mentioned geometry along the height of the heat exchanger channel, a relatively high number of sheet metal plates, n_{sm}, is needed to generate the desired bar height of 12 mm along h_{HX}. For the determination of the uncertainty of the packing void fraction, the large number of plates and their individual manufacturing, such as assembly, uncertainties accumulate according to (21). The sensitivity analysis u_β for the "w12 h12 n3 z15" packing shows a dominant relative variance for the uncertainty of the packing geometry of 82 % see (23), further confirming the approach of using the extended particle hold-up to compare the hold-up behavior between different packing geometries.

$$\left[\left(\frac{\partial\beta}{\partial\epsilon_0}\right)\frac{u_{\epsilon_0}}{u_\beta}\right] = 82\% \tag{23}$$

Fig. 8a shows the same initial geometry set as in Fig. 8b with the extended particle hold-up applied. All structures provide an extended hold-up in the range from $3 \cdot 10^{-3}$ to $3.5 \cdot 10^{-3}$. This relatively narrow band of β^* however spreads over a relative wide range of geometric changes, such as bar-width, -number, -height and also the vertical falling distance, z. To further increase the particle hold-up, additional packing structures were investigated by assembling geometries with the smallest possible vertical spacing, z, and bar height, h_{bar}. Fig. 9 shows the measured hold-up for packing geometries with the smallest possible vertical spacing that can be installed in the designed test rig. By reducing the number of sheet metals per packing layer to $n_{\mathrm{ts}} = 1$, the vertical distance can be further reduced to z = 5 mm for a large number of investigated packings. In addition, for some of these structures, the hold-up was measured for an increased falling height of z = 10 mm, while the "w10 h02 n03", "w12 h02 n03" and "w14 h02 n2" packings could only be measured with a greater vertical distance, since at z = 5 mm particle blocking occurred immediately, causing the entire structure to flood with particles.

Fig. 9 illustrates that packing structures with a relatively high number of bar elements per packing layer ($n \geqslant 5$) for the investigated setup do not lead to a higher particle hold-up than those

Table 2
Overview of conducted experiments.

Experiment	Identifaction of	Varied	Constant
Comparison of different packing geometries without gas flow	Packing with highest hold-up	packing structures	particle flow no air flow
Comparison of different packing geometries with gas flow	Packing with highest hold-up	packing structures air flow	particle flow
Comparison of particle density distribution in packing structures	Packing, providing most even particle distribution	packing structures air flow	particle flow range

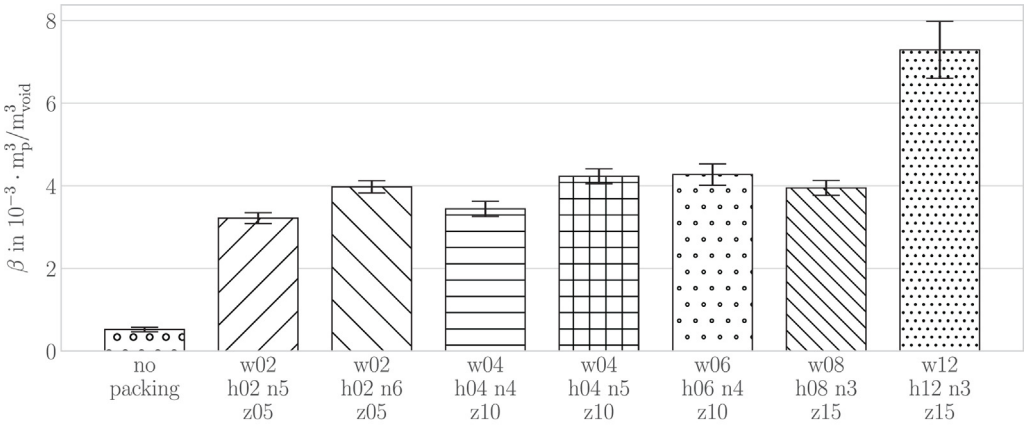

(a) particle hold-up, β

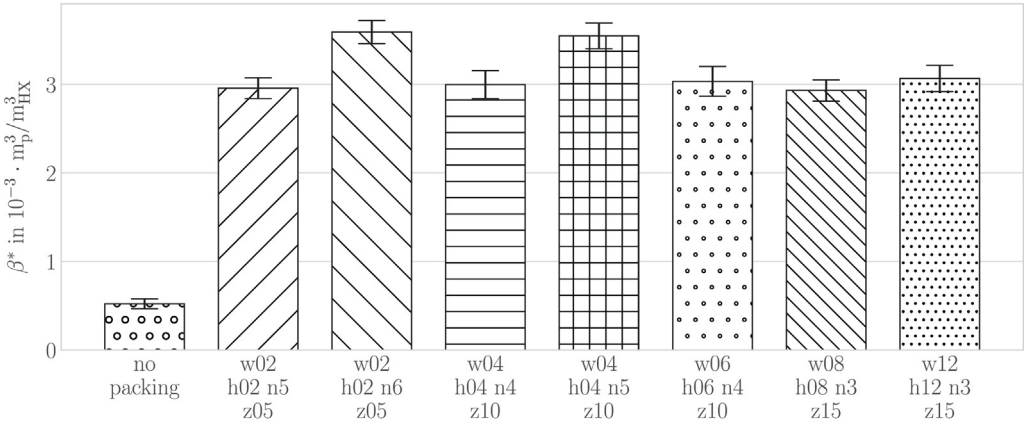

(b) extended particle hold-up, β^*

Fig. 8. Comparison of different packing geometries without gas flow, $\dot{m}_p^{\#} = 2\ \mathrm{kg/(s \cdot m^2)}$.

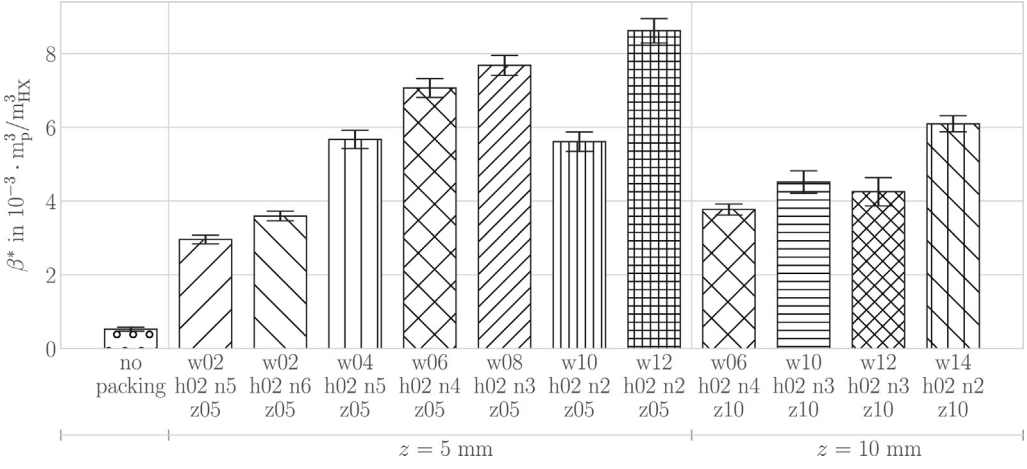

Fig. 9. Extended particle hold-up, with lowest bar height h02, $\dot{m}_p^{\#} = 2\ \mathrm{kg/(s \cdot m^2)}$.

with a lower number ($n < 4$). Very narrow structures represented by "w02 h02 n5 z05" or "w02 h02 n6 z05" provide a relatively low particle hold-up. The hold-up increases as the bar width increases, while the number of bars is gradually reduced to keep the void distance large enough to prevent particles from blocking. Also, the assumption in the previous work of Reichart et al. [12], that a resting particle pile up on the packing structure reduces the mean particle sink velocity, can be strengthened. During the experiments, it was observed that a resting particle layer on the packing surface composed of more than two particle layers has the potential to absorb and dissipate the kinetic energy of the trickling grains, causing a further reduction of the particle sink velocity,

and conversely, increasing the dynamic particle hold-up. Accordingly developed particle piles were observed for bar widths of $w_{bar} \geqslant 6$ mm.

4.2. Comparison of different packing geometries with gas flow

Based on the results shown in Fig. 9, additional countercurrent gas flow tests were conducted with packing geometries ranging in bar widths from 6 mm to 14 mm and a correspondingly adapted number of bars. Fig. 10 depictures the measured hold-ups for varying gas flow rates within the different packing geometries.

With increasing gas flow rates, the measured hold-ups increase until flooding occurs. The transition of the particle flow regime, where flooding of particles within the packing void occurs, can be observed in a steep increase of β^* with $\dot{m}_a^\#$ accompanied by a high relative uncertainty of the measured data points. The w08-packing shows a relative uncertainty of $u_{\beta^*} = 19.7$ % for the highest measured value of β indicating the particle hydrodynamics being close to flooding, while typically u_{β^*} rarely exceeds 3.5 % for measurements sufficiently far from the flooding point. Assuming that the heat capacities of the particles and air are approximately equal, $c_{p,a} \approx c_{p,p}$, and assuming an optimized operating condition of the TFHX with equal heat capacity flow rates, stable operation is preferred for an air flow rate of $\dot{m}_a^\# \approx \dot{m}_p^\# = 2\ \mathrm{kg/(s \cdot m^2)}$. The packing structures with vertical falling distances of $z = 5$ mm cannot be operated up to this airflow without the occurrence of flooding. This was observed for the packings "w12 h02 n2 z05", "w08 h02 n3 z05", and "w06 h02 n4 z05", where no measurement for β^* could be performed for gas flow rates above 0.6 $\mathrm{kg/(s \cdot m^2)}$ and 1.6 $\mathrm{kg/(s \cdot m^2)}$, respectively. By increasing z to 10 mm, the measured hold-ups are reduced. This was already illustrated in Fig. 9, as the particles can accelerate to higher falling velocities due to the increased vertical distance between the packing layers. The geometries "w10 h02 n3 z10", "w12 h02 n3 z10", and "w14 h02 n2 z10" exhibit stable flow conditions for the preferred air flow rate and beyond, from those the w10-packing provides the highest particle hold-up. The w12-packing shows similar hold-up performance up to 2 $\mathrm{kg/(s \cdot m^2)}$ air flow, while the w14-type provides the lowest retention of trickling particles in the HX.

4.3. Comparison of particle density distribution in packing structures

The three last mentioned geometries provide all good particle retention. To further identify the most suitable packing structure, the mixing quality of the packing "w10 h02 n3 z10" and the packing "w14 h02 n2 z10" was directly compared. Therefore, in separate experiments observation areas in the packing structures were created and videos of the particle flow with different air and mass flow rates were recorded to determine the relative linear particle distribution, u_{rel}, described in Section 2.3.

Fig. 11 shows the corresponding determined experimental mean values of $\bar{u}_{rel}$ for each packing at varying flow conditions. Air mass flow rates ranging from 0 $\mathrm{kg/(s \cdot m^2)}$ to 9 $\mathrm{kg/(s \cdot m^2)}$ were investigated. In addition, three orifice plates with different diameters were installed to obtain different exemplarily particle mass flow rates for the measurements. It was observed that for one orifice plate the resulting particle mass flows are not constant, but decrease with increasing air mass flow rates, see Table 3. Accordingly, only ranges of particle mass flows can be provided for the results in Fig. 11.

The origins of this observation are not yet fully understood and should be investigated in more detail in future work. What can be observed is that a narrower orifice, with a diameter closer to a critical diameter where particle blocking is more likely to occur, shows a greater sensitivity to an increased air flow of the resulting particle mass flow.

Fig. 11 shows that a packing structure with an increased bar width of 14 mm results in a measurable deterioration of particle mixing quality. The effect of increased particle shaded areas was measured. For both packing structures an enhancement of particle mixing with increasing air flow was observed for air flow rates beyond 4 $\mathrm{kg/(s \cdot m^2)}$. By surpassing flow rates of 8 $\mathrm{kg/(s \cdot m^2)}$ and thus entering the range of the particle terminal velocity at ambient temperature, the hydrodynamics of the particles start to change from a trickling state to a fluidized state, resulting in mixing qualities close to ideal stochastic uniform mixing. Since the blower used in the presented setup was not able to provide higher air flow rates than 9 $\mathrm{kg/(s \cdot m^2)}$, no data for air mass flow rates higher than this is available. By assessing the particle hold-up and the particle distribution in all conducted experiments, the

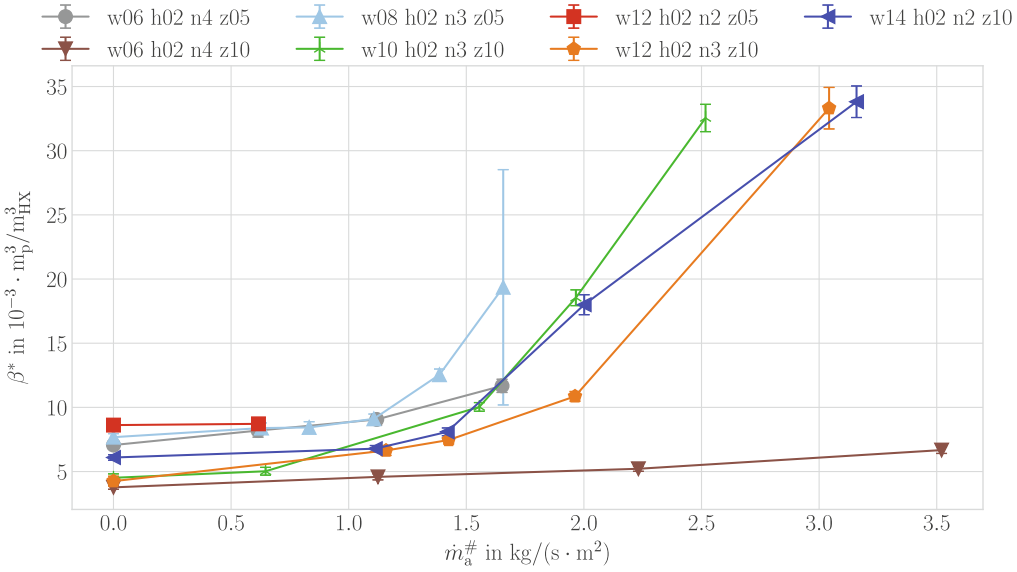

Fig. 10. Extended particle hold-up vs. gas flow for varying geometries, $\dot{m}_p^\# = 2\ \mathrm{kg/(s \cdot m^2)}$.

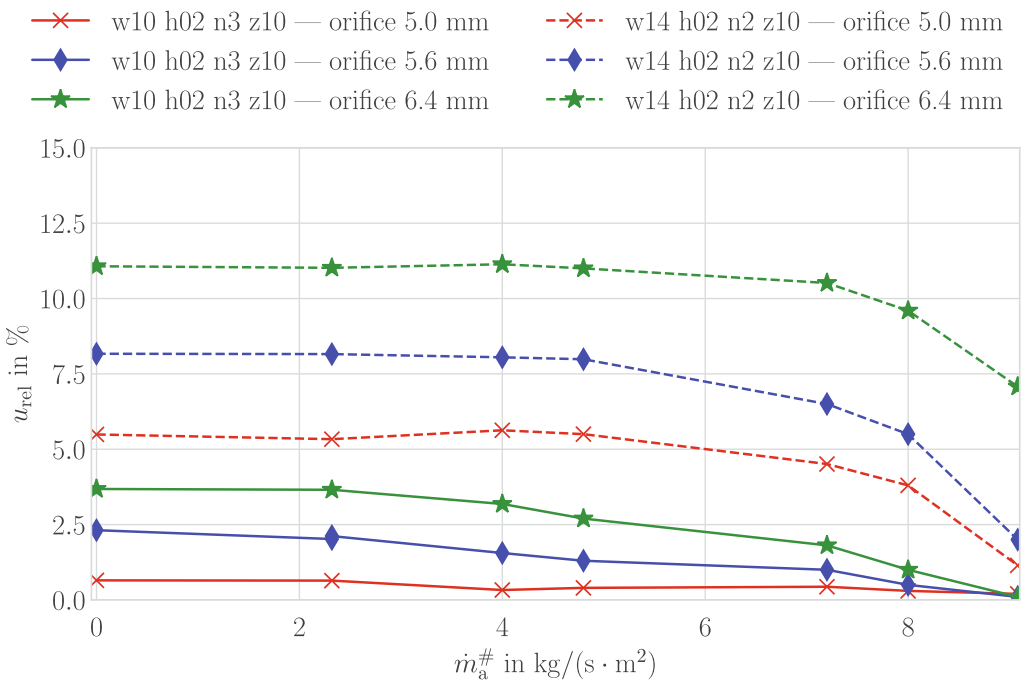

Fig. 11. Relative, linear particle distribution in two packing geometries, for varying air and particle mass flow rates.

Table 3
Resulting particle mass flow rates in kg/(s · m²) for different orifice diameter and air flow rates.

	Orifice diameter mm		
air flow kg/(s · m²)	5.0	5.6	6.4
0	1.5	1.9	2.7
9	0.6	1.4	2.3

"w10 h02 n3 z10" packing structure was identified to be the most suitable geometry for the chosen setup. It provides the desired requirements of the particle hydrodynamic for the used particles within a TFHX and will be used in further hot test to evaluate the heat transfer performance of the system.

5. Conclusion and outlook

Experimental cold tests were conducted with the objective of identifying a suitable packing geometry that would provide a high particle hold-up at stable flow regimes for a trickle flow heat exchanger. Based on previous work, it was decided to use packing structures consisting of regular arrangements of rectangle bar elements. A test setup was developed and described, capable of assembling different packing geometries. The extended particle hold-up, β^*, was used to compare packing structures with different geometrical dimensions. It was demonstrated that the particle hold-up decreases as the vertical falling height between two successive packing layers increases. Additionally, it was observed that a small bar width and a high number of bars do not result in a higher dynamic particle hold-up. For the particles in question, bar widths of 6 mm and above proved to be optimal in providing sufficient width to accumulate a pile of static particles, capable of absorbing the kinetic falling energy of the trickling particles and reducing the mean particle sink velocity by increasing the dynamic particle hold-up. However, the bar width should not be chosen excessively wide to prevent the influence of particle shadowing, which would result in a reduced quality of spatial particle distribution. A packing structure with w_{bar} = 10 mm, h_{bar} = 2 mm, n_{bar} = 3 and z = 10 mm was identified for the used particles. This geometry provides stable operating conditions and the highest dynamic particle hold-up within the desired media flow rates at a relatively uniform spatial particle density distribution. In future work, the identified packing will be tested with hot air flow. The influence of varying air and particle flow rates, including different media inlet temperatures, will be employed to ascertain the heat transfer performance of the developed TFHX. Particularly in high temperature applications exceeding 400 °C, it is anticipated that the packing structure will exert a positive influence, given that the volume specific surface area of the particles, a_p, and the packing structure, a_{pac}, are of a comparable magnitude [12]. Particles with high temperatures, for instance, those originating from a CST receiver, would enter a TFHX and heat the packing structure through thermal radiation. Consequently, the heat transfer in the high-temperature zone of the TFHX would not only occur between air and particles, but also between air and the packing. This would result in an increased surface area involved in the heat transfer, thereby increasing the power density of a gas-particle TFHX. The results of the aforementioned experiments will serve as a foundation for the calibration of models designed to predict and scale heat exchangers that are appropriate for future applications.

Declaration of Competing Interest

The authors declare that they have no known competing financial interests or personal relationships that could have appeared to influence the work reported in this paper.

Acknowledgment

The presented results have been elaborated as part of the PREMA-project, funded from the European Union's Horizon 2020 Research and Innovation Programme under Grant Agreement No. 820561.

References

[1] Miriam Ebert, Lars Amsbeck, Andrea Jensch, Johannes Hertel, Jens Rheinländer, David Trebing, Ralf Uhlig, Reiner Buck, Upscaling, Manuf. Test of a Centrifugal Particle Receiver. (2016). https://doi.org/10.1115/ES2016-59252.

[2] Miriam Ebert, Lars Amsbeck, Jens Rheinländer, Bärbel Schlögl-Knothe, Stefan Schmitz, Marcel Sibum, Ralf Uhlig, Reiner Buck, Operational experience of a centrifugal particle receiver prototype, AIP Conf. Proc. 2126 (1) (2019) 8. https://doi.org/10.1063/1.5117530, URL ISSN 0094-243X. https://aip.scitation.org/doi/abs/10.1063/1.5117530.

[3] Chang-he Gao, Peng Jiang, Yong Li, Jia-lin Sun, Jun-jie Zhang, Huan-ying Yang, One step sintering of homogenized bauxite raw material and kinetic study, Int. J. Miner., Metall., Mater. 23 (10) (2016) 1231–1238. https://doi.org/10.1007/s12613-016-1343-8.

[4] J.H.A. Kiel, W. Prins, Willibrordus Petrus Maria van Swaaij, Modelling of non-catalytic reactors in a gas-solid trickle flow reactor: Dry, regenerative flue gas desulphurization using a silica-supported copper oxide sorbent, Chem. Eng. Sci. 47(17):15 (1992). https://doi.org/10.1016/0009-2509(92)85105-K, ISSN 0009-2509.

[5] Daizo Kunii, Octave Levenspiel, Fluidization engineering, Butterworth-Heinemann series in chemical engineering, 2nd edition., Butterworth-Heinemann, Boston, 1991, ISBN 0409902616 9780409902617 0409902330 9780409902334.

[6] J.F. Large, P. Guignon, and Estéban Saatdjian. Multistaging and solids distributor effects in a raining packed bed exchanger. 1983.

[7] Claus Maarup, Gas-Solid Heat Exchanger for Cement Production, Dissertation (2013), URL https://pdfs.semanticscholar.org/04e3/cd1921e99be6451ef40772d5762736a0077a.pdf.

[8] K. Nagata, H. Ohara, Y. Nakagome, Y. Hamada, Y. Bando, M. Nakamura, S. Toyama, The heat transfer performance of a gas-solid contactor with regularly arranged baffle plates, Powder Technol. 99 (3) (1998) 302–307. https://doi.org/10.1016/s0032-5910(98)00127-2, ISSN 0032-5910. URL <Go to ISI>://WOS:000076344300012.

[9] N.M. Nikacevic, M. Petkovska, and M.P. Dudukovic. Solids flow pattern in gas-flowing solids-fixed bed contactors. part i experimental. Chem. Eng. Sci., 64 (10), 2501–2509, 2009. doi:10.1016/j.ces.2009.02.029. ISSN 0009-2509. URL <Go to ISI>://WOS:000266114200023.

[10] I.W. Noordergraaf, W.P.M. van Swaaij, and A.W.M. Roes. Axial mixing and mass transfer in a zig-zag contactor. 1980. ISSN 0306404583 (ISBN); 9780306404580 (ISBN). https://www.scopus.com/inward/record.uri?eid=2-s2.0-85040280254&partnerID=40&md5=daeb56c6f40ab9730dc325d73c4b8ff7.

[11] I.W. Noordergraaf, A.B. Verver, W.P.M. Van Swaaij, Gas/feststoff-rieselstromung und austauschprozesse in einem zickzack-kontaktor, SPRECHSAAL 114 (1981) 3.

[12] Markus Reichart, Martina Neises-von Puttkamer, Reiner Buck, Robert Pitz-Paal, Numerical assessment of packing structures for gas-particle trickle flow heat exchanger for application in csp plants, in: ASME 2021 15th International Conference on Energy Sustainability:7, 2021. doi:10.1115/es2021-62746. doi:10.1115/ES2021-62746.

[13] A.W.M. Roes, Willibrordus Petrus Maria Van Swaaij, Hydrodynamic behavior of a gas-solid counter-current packed column at trickle flow, Chem. Eng. J. 17 (1979) 81–89. https://doi.org/10.1016/0300-9467(79)85001-7.

[14] Estéban Saatdjian, J.F. Large, Heat transfer simulation in a raining packed bed exchanger, Chem. Eng. Sci. 40 (1985) 693–697. https://doi.org/10.1016/0009-2509(85)85021-1.

[15] Saint-Gobain-Proppants. Ultraprop/ sintered bauxite high strength proppants, October 2014 2014. URL www.proppants.saint-gobain.com.

[16] Robert Stieglitz, Volker Heinzel, Thermische Solarenergie: Grundlagen, Technologie, Anwendungen. Springer Vieweg, Berlin, 2012, ISBN 9783642294754, doi:10.1007/978-3-642-29475-4. https://www.tib.eu/de/suchen/id/TIBKAT%3A74085741X.

[17] Matthias Stieß. Partikeltechnologie. Mechanische Verfahrenstechnik. Springer, Berlin; Heidelberg, 3., vollst. neu bearb. aufl. edition, 2009. ISBN 3-540-32551-4 978-3-540-32551-2 978-3-540-32552-9 (Online-Ausgabe). URL http://swbplus.bsz-bw.de/bsz252947673inh.htm.

[18] e.V. VDI (Ed.), Heat Atlas, VDI-Gesellschaft Verfahrenstechnik und Chemieingenieurwesen, VDI-Buch, Springer, Heidelberg, Berlin, 2010. https://doi.org/10.1007/978-3-540-77877-6, ISBN 978-3-540-77877-6.

[19] A.B. Verver, W.P.M. Van Swaaij, The heat-transfer performance of gas—solid trickle flow over a regularly stacked packing, Powder Technol. 45 (1986) 133–144. https://doi.org/10.1016/0032-5910(66)80005-0.

[20] A.B. Verver, W.P.M. van Swaaij, The hydrodynamic behaviour of gas—solid trickle flow over a regularly stacked packing, Powder Technol. 45 (2) (1986) 119–132. https://doi.org/10.1016/0032-5910(66)80004-9, ISSN 0032-5910. URL http://www.sciencedirect.com/science/article/pii/0032591066800049.

[21] A.B. Verver, Willibrordus Petrus Maria van Swaaij, The gas-solid trickle-flow reactor for the catalytic oxidation of hydrogen sulphide: a trickle-phase model, Chem. Eng. Sci. 42 (3) (1987) 435–445. https://doi.org/10.1016/0009-2509(87)80006-4, ISSN 0009-2509.

[22] Klaas Roel Westerterp and Michal Kuczynski. Gas-solid trickle flow hydrodynamics in a packed column. Chemical Engineering Science, 42 (7):1539–1551, 1987. doi:10.1016/0009-2509(87)80159-8. ISSN 00092509 (ISSN). URL https://www.scopus.com/inward/record.uri?eid=2-s2.0-0023209227&doi=10.1016%2f0009-2509%2887%2980159-8&partnerID=40&md5=ec6ddac496fb972664 de1f1f27ca3bb7.

[23] C.R. Woodcock, J.S. Mason, Bulk Solids Handling: an Introduction to the Practice and Technology. (1988). https://doi.org/10.1007/978-1-4757-1358-9, ISBN 978-1-4757-1358-9. URL https://link.springer.com/book/10.1007/978-1-4757-1360-2.